Poplar wood and tea biochars for trichloroethylene remediation in pure water and contaminated groundwater

Loïc Della Puppa, Marion Ducousso, Nicolas Batisse, Vincent Verney, Marc Dubois, Vincent Xavier, Florence Delor-Jestin

Poplar wood and tea biochars for trichloroethylene remediation in pure water and contaminated groundwater

Loïc Della Puppa[a], Marion Ducousso[a], Nicolas Batisse[a], Marc Dubois[a], Vincent Verney[a], Vincent Xavier[b] and Florence Delor-Jestin[a*]

[a] *Université Clermont Auvergne, CNRS, SIGMA Clermont, Institut de Chimie de Clermont-Ferrand, F-63000 Clermont–Ferrand, France*

[b] *VTGreen, ZA Les Tiolans, F-03800 Saint-Bonnet-de-Rochefort, France*

[*]corresponding author: florence.delor_jestin@sigma-clermont.fr

Abstract

Four biochars from pyrolysis of poplar wood (biochar P) and tea (biochar T) at 450 and 750°C have been tested in a first time as adsorbents for trichloroethylene (TCE) removal in groundwater. The physico-chemical properties of biochars were systematically investigated with organic elemental analyser, scanning electron microscopy, N_2 adsorption measurement, IR spectroscopy and X-ray photoelectron microscopy. Three kinetic models were used to follow the TCE removal by biochars. The best kinetic performances were obtained with biochars P with the smallest particle size diameter (50 – 100 µm) due to their porosity and the mass transfer limitation for the TCE remediation. Remediation of a real sample of groundwater polluted by chlorinated organic compounds showed that biochar P produced at 750°C is more efficient to remove vinyl chloride (65% adsorbed) than commercial activated carbon powder (40%). The TCE sorption capacity is similar in pure water and in polluted groundwater. The results also highlighted better retention capacity for the most substituted molecules (tri and tetrachloroethylene) for biochar P750.

Keywords: biochars, organic contaminants, sorption kinetics, water pollution remediation.

Abbreviations:

Biochar P: poplar wood biochar (P750, produced at 750°C)

Biochar T: tea biochar

Cl-VOC: Chlorinated Volatile organic compound

IPD: Intra-particle diffusion model

PFO: Pseudo-first order

PSO: Pseudo-second order

TCE: trichloroethylene

Highlights:

- The biochar with the smallest particle size exhibits higher kinetic performances
- Poplar wood biochar can be a promising adsorbent
- The trichloroethylene sorption capacity is the same in pure and polluted waters
- Biochar presents higher vinyl chloride remediation than an activated carbon

1. Introduction

Organic contamination represents a serious threat for both the human health and the environment (Genthe et al., 2018; Loflen et al., 2018; Zhang et al., 2017). Due to a rapid and massive worldwide industrialisation, pollutants bioaccumulate in soils, surface waters and ground waters in addition to presenting a high toxicity (Khan et al., 2009; Kushwaha et al., 2018; Trama-Freitas et al., 2017). Different technologies have been developed for the treatment of contaminated water such as filtration, flocculation, ion exchange resins, evaporation, membrane processes, adsorption, etc. Among all the potential sorbent, activated carbons exhibit a valuable pollutant removal capacity and an important versatility (Erto et al., 2010; Largitte and Pasquier, 2016; Lian et al., 2012). Hence activated carbons is considered as a reference for the water pollution remediation, several reviews approached the use of low-cost adsorbents to replace the activated carbons with the double objectives of giving to green wastes such as agricultural waste a second life while decreasing the cost of water and wastewater treatments (Ali et al., 2012; De Gisi et al., 2016). One of the main issues however is to ensure consistent performances over time since one has to deal with a large variability of green waste composition and properties.

Much attention on the biochar which is a solid residue from the thermal-conversion (roasting, pyrolysis, gasification) of various biomasses. Biochars are carbonaceous materials potentially porous and containing a non-negligible amount of minerals (Ca, Na, K, Mg). The advantage of this materials is its cost and the possible adjustment of the surface properties (surface functionalities, porosity, surface acidity) by the selection of the feedstock and the production process (Ahmad et al., 2012; Yaashikaa et al., 2019). Different studies already proved the biochar remediation capacity for aqueous solutions (Ahmad et al., 2014; Tan et al., 2015; Saleh et al., 2016). The biochars remediation mechanisms depends on both the biochar and

the pollutant. In the case of a non-polar organic compounds as trichloroethylene (TCE), the contaminant interacts with hydrophobic sites of the biochar surface in the absence of H-bonding between water and O-containing functional groups (Ahmad et al., 2014; Sigging et al., 2020). TCE is a carcinogenic and mutagenic chlorinated volatile organic compound (Cl-VOC). Its accepted upper level is fixed at 5 μg L^{-1} in the drinking water (Luo et al., 2016) and its pollution sources are mainly the textile, refrigeration, metal industry degreasing, lubricants and adhesives industries. TCE remediation is difficult due to its intrinsic characteristics since it is a volatile compound with a moderate solubility. The TCE sorption capacity in various environments (pure and real polluted water) is not given.

In the present study, biochars were produced at 450°C and 750°C from poplar wood and tea waste. For the first trials, biochars have been examined for the treatment of TCE in pure water. The emphasis will be put on the effect of the feedstock, pyrolysis temperature and particle size on the kinetic sorption. Then for the latest trials, the most efficient biochar was tested and compared with a commercial activated carbon over a chlorinated polluted groundwater. The TCE sorption capacity will be determined und underlined in various environments.

2. Materials and methods

2.1. Biochars production and characterisation

Poplar wood biochar samples (referred as biochar P) and tea biochar samples (referred as biochar T) were provided by VTGreen Inc. (Saint Bonnet de Rochefort, France). Biochars was produced by the patented process Biogreen® using the Spirajoule® technology. Biogreen® is one of the leading pyrolysis process in Europe, developed since 2003. A module is designed to process up to 2.5 m^3/hr. Mass capacity is linked to the treatment time of biomass and the density. Briefly, the biomass is continuously introduced into the reactor and conveyed along the pyrolysis chamber thanks to a heated worm screw conveyor with a residence time fixed at 15 min. Biochars were firstly produced at 450°C (P450 and T450) and 750°C (P750 and T750).

Elemental composition (C, H, N, S, O) was performed on 1 g of dried sample using an organic elemental analyser (Thermo Scientific^{TM} Flash 2000). The ash content was determined by heating 1 g of sample up to 550°C with a 5°C/min heating rate. The particle size distribution was realised on 15 g of biochars using a set of sieves (50 to 2000 µm mesh). Biochar morphology was investigated using scanning electron microscopy SEM (SH400M, Hirox). The porous structure of the biochars was examined on an ASAP 2020, Micromeritics (USA) by N_2 adsorption at 77 K. From the N_2 adsorption isotherm, the specific surface area (SSA) and the pore distribution were determined using respectively the BET equation and the DFT method. All the samples were outgassed at 300°C for 720 min prior to the measurements. FTIR spectra were generated by implementing the attenuated total reflection (ATR) method. IR spectra were collected between 500 and 4000 cm^{-1} with a resolution of 4 cm^{-1}. The X-ray photoelectron microscopy (XPS) were performed on a Kratos Analytical AXIS Ultra DLD spectrometer using polychromatic Al Kα X-ray radiation (1486.6 eV) with pass energy of 20 eV. All survey and high-resolution scans were realised with the neutraliser and all samples were incrusted onto Indium foil.

The pH of the biochar was measured using a 1/2.5 w/v ratio with either ultra-pure water or 1 M KCl (ISO 10390). Point of zero charge (pH_{ZPC}) was measured using the immersion technique (Fiol and Villaescusa, 2009). It consisted in adding 0.75 g of biochar to 30 mL of 0.03 M KNO_3 solution sets at different pH values under agitation for 24h. The pH_{ZPC} was the pH at which the difference between the initial and the final pH values was the lowest. The

cationic exchange capacity (CEC) was measured according to the Metson method (NF X31 130). Briefly, 10 g of sample is saturated in NH_4^+ using a 1 M ammonium acetate pH 7 solution. The sample is then washed with 100 mL of ethanol to removed ammonium excess. The sample is then percolated with 250 mL of 0.1 M NaCl. The NH_4^+ distilled and recovered in a sodium hydroxide solution is then titrated using a 0.1 M H_2SO_4 solution.

2.2. Sorption experiments

TCE (99.5%) was purchased from Sigma-Aldrich. Ultra-pure water from Millipore Milli-Q system (resistivity 18 MΩ cm, DOC < 0.1 mg L^{-1}) was used for the solutions preparation.

A stock solution of TCE (500 mg L^{-1}) was prepared using ultra-pure water and agitated overnight. Kinetic experiments were performed using a 20 mg L^{-1} solution and a w/v ratio of 1/700 in amber flask with no headspace to avoid TCE photodegradation and evaporation (50 mg of biochar and 40 mL of TCE solution). Concerning the sorption isotherm, they were performed using an equilibrium time of 24h. The flasks were agitated with magnetic stirrers at 250 rpm and a flask was sacrificed for each measurement time. Aliquots were filtered through 0.45 µm PTFE filters and stored at 4°C with no headspace before analysis.

Adsorption tests were also performed on a groundwater sample contaminated by various chlorinated volatile organic compounds (Cl-VOCs) (Table 1) and supplied by Biobasic Environnement Inc. (Saint - Beauzire, France). The sample is a contaminated industrial real groundwater. Activated carbon (Norit SAE Super activated carbon powder from Cabot company) was used as a comparison. The activated carbon powder presented an apparent density of 25 kg m^{-3}, a specific surface area of 1050 m^2 g^{-1} with mainly meso- and macro-porosity and a particle size of 90 µm.

Table 1: List of the chlorinated pollutants in the real groundwater, their abbreviations, log Kow, concentration (µg L^{-1}) in the water sample and their respective molar volume (cm^3).

Pollutants	Abbreviation	Structure	Log K_{ow}[1]	Molar volume	Concentration
Dichloromethane	DCM	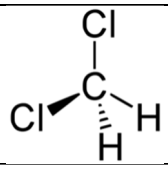	1.25	67.8	1300
Trichloromethane	TCM	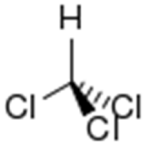	1.97	79.5	130
1,1-dichloroethane	1,1-DCA	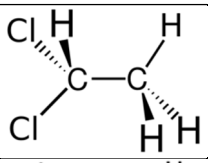	1.79	84.6	520
1,2-dichloroethane	1,2-DCA	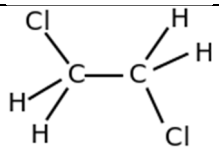	1.48	84.3	550
1,1,1-trichloroethane	1,1,1-TCA	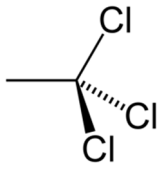	2.49	95.7	57000
Vinyl chloride	CV	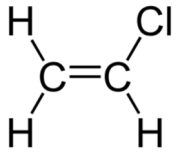	1.46	68.0	550
1,2-cis-dichloroethylene	cis 1,2-DCE	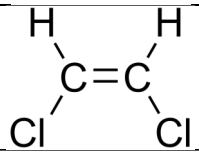	1.86	77.9	96000
1,1-dichloroethylene	1,1-DCE	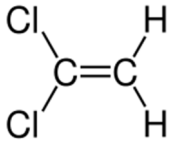	2.13	79.2	2900
Trichloroethylene	TCE	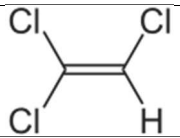	2.61	89.1	41000
Tetrachloroethylene	PCE	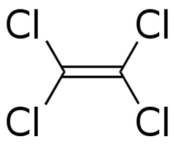	3.40	100.3	4900

2.3. Analysis

The TCE concentration was determined using a high-performance liquid chromatography (LC-10AT Shimadzu) – UV detection equipped with a C18 column (EC 250/4 NUCLEOSIL 100-5 from Macherey Nagel). The samples injected (10 µL) were eluted with a mixture of acetonitrile and water (85:15) at 1.0 mL min^{-1}. The TCE absorbance was measured at 198 nm. Polluted groundwater samples were analysed by GC-MS (6890N Agilent) according to the NF EN ISO 10301.

2.4. Sorption models

Three kinetic models were introduced for the data interpretation: (1) the pseudo-first order (PFO), (2) the pseudo-second order (PSO) and (3) intra-particle diffusion model (IPD):

(1) $$q_t = q_e\,(1 - e^{-k_1 t})$$

(2) $$q_t = \frac{k_2 q_e^2 t}{1 + k_2 q_e t}$$

(3) $$q_t = k_{id} t^{0.5} + \theta$$

Where k_1 (min^{-1}), k_2 (g $mmol^{-1}$ min^{-1}) and k_{id} ($min^{-0.5}$) represent the kinetic constants of respectively PSO, PFO and IPD models, q_e and q_t (mmol g^{-1}) the amount adsorbed at equilibrium and at time t (min) and θ a constant related to the intra-particular diffusion model.

The sorption isotherm data were fitted to the Langmuir isotherm (4) as follows:

(4) $$S = \frac{S_{max} K C}{1 + K C}$$

Where S_{max} denotes the maximum sorption capacities, K the Langmuir constant and C the concentration of TCE in solution. The Langmuir parameters was obtained from the Bolster and Hornberger (2007) spreadsheet.

3. Results and discussion

3.1. Biochars characterisation

SEM images of the different biochars presented different morphology with irregular shapes depending on the raw feedstock (Fig. 1). Whereas biochar originating from tea feedstock are more strip-like shapes (T450 and T750), biochar originating from poplar wood feedstock presents irregular porous shapes (P450 and P750). No significant differences appear between biochar produced at different pyrolysis temperature.

Properties of the biochars are given in Table 2. Their chemical compositions differ depending on the raw feedstock and the pyrolysis temperature. The biochar P750 present the highest carbon content (94.7%) whereas its oxygen content is the lowest (4.3%). Increasing the pyrolysis temperature decreases the atomic H/C and O/C ratio of the biochars due to carbon graphitisation into well-organised layers associated with a dehydration and a deoxygenation of the biochar, which is consistent with the literature (Ahmad et al., 2014; Bogusz et al., 2015; Li et al., 2017). The evolution of the H/C ratio gave indications about the carbonisation and aromaticity of the biochars whereas the decrease of the O/C ratio results in an increase of the hydrophobicity of the biochars (Mohammed et al., 2018). The ash increases along with the pyrolysis temperature. Biochars T exhibited higher ash amount compared to biochar P which indicate that they present a higher inorganic content.

Table 2: Elemental composition, molar atomic ratio, ash content in dry sample, specific surface area (SSA), total pore volume (V_{tot}), pH_{H2O}, pH_{KCl}, pH of zero-point charge (pH_{ZPC}) and cation exchange capacity (CEC) of the studied biochars.

	Elemental composition (wt.%)					Atomic ratio		Ash	pH_{H2O}	pH_{KCl}	pH_{ZPC}	CEC
	C^a	H^a	O^a	N^a	S^a	H/C	O/C	(wt.%)				(meq kg^{-1})
P450	84.7	2.9	12.1	0.2	0	0.41	0.11	5.4	8.9	8.4	9.0	40
P750	94.7	0.8	4.3	0.2	0	0.10	0.03	5.6	11.2	9.9	10.5	10
T450	72.6	3.7	19.1	4.6	0	0.61	0.20	13.7	9.4	8.6	8.5	68
T750	83.5	1.4	11.5	3.6	0	0.20	0.10	14.9	12.2	9.8	10.5	7.4

[a] ash and moisture free

All biochars exhibit an alkaline pH that increases with the pyrolysis temperature. This increase is possibly due to the alkali salts separation from the organic matrix (Trakal et al., 2014). Furthermore, as shown in Table 2, Biochar T450 presents the higher CEC (68 meq kg^{-1}) possibly due to its higher O content, the CEC being strongly dependent from the O-

containing groups content (carboxylic acids, hydroxides, ect.) (Harvey et al., 2011). The decrease of the O-containing groups could also explain the decrease of the CEC with the pyrolysis temperature increase.

Table 3: Specific surface area (SSA), total pore volume (V_{tot}), micropore volume (V_{micro}), mesopore volume (V_{meso}) and distribution of biochar particle size between <50 µm and 2000 µm.

	SSA	V_{tot}	V_{micro}	V_{meso}	Particle size distribution (%)				
	(m^2 g^{-1})	(cm^3 g^{-1})	(cm^3 g^{-1})	(cm^3 g^{-1})	< 50	50 - 100	100 - 500	500 - 1000	1000 - 2000
P450	91.4	0.04	0.03	0.01	0	0.7	30.0	49.8	19.5
P750	341.0	0.14	0.13	0.01	1.7	8.5	48.6	32.4	8.8
T450	3.3	-	-	-	0	2.1	34.7	45.8	17.4
T750	5.3	-	-	-	0	2.5	53.8	38.2	5.5

The SSA, pore volume and particle size distribution are presented in Table 3. Pore size distribution for P450 and P750 are shown in Fig. S1, no results are however presented for T450 and T750 as they are low porosity materials. Biochar P450 exhibits a SSA of 91.4 m^2 g^{-1} and a total pore volume of 0.04 cm^3 g^{-1}. At a higher pyrolysis temperature (from 450 to 750°C), pore development is more important since SSA and total pore volume reach 341.0 m^2 g^{-1} and 0.14 cm^3 g^{-1} respectively for P750. This increase is possibly due to the exposure of the aromatic lignin core, the higher the pyrolysis temperature the higher the pore development (Ahmad et al., 2014). In fact, Lehmann (2007) reported an optimal pyrolysis temperature range (i.e. 450-550°C) for the specific surface development of biochars produced from the pyrolysis of dried wood *Robinia Pseudacacia*. This optimal pyrolysis temperature is however highly dependent from the biomass feedstocks and the pyrolysis operating conditions. As a direct example, the two biochars T (produced at 450 and 750°C) have a low SSA (being lower than 5 m^2 g^{-1}). Porosity distribution shows that micro porosity increases in the biochar structure with an increase of the pyrolysis temperature. For P450, micropores represent 75% of the total pore volume whereas they represent 93% for P750. This increase can be related to the decrease of the particle size. It is also noticeable that the particles size is smaller than 2000 µm with 80% of the particles in the range 100 - 1000 µm. An increase of the pyrolysis temperature tends to decrease the particles size.

As shown in the FTIR spectra (not shown, see Additional data), the biochars produced at 450°C present similar patterns with typical peaks at 1160 cm^{-1} (C-O stretch), at 1590 cm^{-1}

(C=C stretching in aromatic ring) and at 1690 cm^{-1} (C=O stretching) (Lam et al., 2016; Smith et al., 2016). The decrease in the number of spectral features when increasing the pyrolysis temperature is also visible due to the graphitisation of the biochars and to the dehydration and deoxygenation during the process. This associated with the decreased in the oxygen content (Table 2) can explain the disappearance of the functional group peaks in the FTIR spectra for a same biomass feedstock.

The difference in surface properties observed on FTIR spectra are also confirmed by the high-resolution C1s and O1s XPS spectra (Fig. 2). The C1s peak was deconvoluted into three peaks representing C-C/C-H at 284.5 eV, C-O at 286.2 eV and C=O at 288.4 eV. The deconvolution of O1s peak results into three peaks at 531.1 eV (=O), 532.5 eV (-O) and 533.7 eV (-OH provided by physisorbed water). The C1s spectra show that biochars produced at the same temperature present similar distribution. It is moreover noticeable that the increase of the pyrolysis temperature results in an augmentation of the C-C/C-H relative content and in the decrease of oxygen-bearing functional groups (C-O and C=O), which is in accordance with FTIR spectra and O/C atomic ratio (Table 2). Concerning the O1s XPS data, biochar from poplar wood and tea present different distribution with higher density of =O group for T450. When increasing the temperature, the O1s tends to the same distribution, which is in agreement with results observable in the literature (Smith et al., 2016).

3.2. TCE sorption

3.2.1. Influence of the precursors type and the pyrolysis conditions on TCE remediation

The sorption experiments allowed to determine the removed concentrations of TCE with liquid chromatography. TCE adsorption kinetics with PFO and PSO models are then proposed. Fig. 3 shows the effect of contact time on the removal of TCE for the biochars P and T produced at 450°C and 750°C. The sorption kinetics can be decomposed into two phases: a fast step of 25 min followed by a relatively slow phase. This behaviour is commonly observed and is due to the availability of the sorption site which become less available and saturated (Ahmad et al., 2013a) . The poplar wood feedstock biochars are more efficient for TCE removal than tea biochar. The TCE sorption on biochars T reached the equilibrium at

160 min, removing 40% of the initial TCE while on biochars P, the equilibrium is attained only after 50 min with 98% of the TCE sorbed. Compared to biochar produced at higher pyrolysis temperature, no significant differences in the efficiency appear. The kinetic parameters resulting from the application of pseudo-first order (PFO), pseudo-second order (PSO) and intraparticle diffusion (IPD) model are presented in Table 4.

Table 4: kinetic parameters for the TCE removal by biochars P450, P750, T450 and T750.

		PFO			PSO			IPD
TCE	q_{exp}	k_1	q_e	R^2	k_2	q_e	R^2	R^2
P450	0.101	0.065	0.073	0.9541	2.12	0.104	0.9990	0.6298
P750	0.100	0.022	0.071	0.8644	0.59	0.103	0.9989	0.5572
T450	0.040	0.022	0.036	0.9682	0.93	0.043	0.9932	0.8370
T750	0.045	0.012	0.041	0.9641	0.23	0.056	0.8923	0.9047

q_{exp} and q_e: mmol g^{-1} k_1: min^{-1} k_2: g $mmol^{-1}$ min^{-1}

TCE data are globally well fitted by PFO and PSO, indicating that both physisorption and chemisorption are involved in the sorption mechanisms. The experimentally determined amount of TCE sorbed by the biochars are however better estimated using the PSO indicating that more than one sorption mechanisms are involved. Moreover, it is also noticeable a decrease in kinetic constant when increasing the pyrolysis temperature. This phenomenon was already observed by Ahmad et al. (2013a). However, in the case of phenol adsorption on pine fruit shells biochar, the kinetic constant increase along with the pyrolysis temperature (Mohammed et al., 2018). This indicates that the trend seems to depends of the biochar properties as the surface composition, the SSA and the pore volume distribution of the biochars at the different pyrolysis temperature.

The sorption can however also be limited by the intraparticle diffusion. As shown in additional data, the IPD model can describe the TCE sorption on the biochars. However, when the data can be fitted with two straight lines (P450 and P750), this indicates that macropore and mesopore diffusion occur in a first place followed by micropore diffusion (Fierro et al., 2008). Results show that biochars from poplar wood are more efficient for TCE removal than tea biochars. Surface properties are one of the main reasons of this efficiency. The mechanisms involved are the electrostatic attraction, polar organic attraction, non-polar organic attraction and partition in non-carbonised phase (Ahmad et al., 2014). These

mechanisms are directly dependent on the biochar surface properties as the surface polarity, aromaticity, type and number of functional groups. As a non-polar compound, TCE retention is mostly affected by the biochar SSA, porosity and the carbon extent (Schreiter et al., 2018). As presented in Table 3, biochars P present a higher carbon content (84.7 to 94.7 wt%) than biochars T (72.6 to 83.6 wt%) but more importantly, biochars P are porous sorbents with a SSA higher than 90 m^2 g^{-1} while biochars T have low porosity.

It is also interesting to examine the influence of the pyrolysis temperature on the biochars adsorption efficiency. Ahmad et al. (2013a) showed that an increase of the pyrolysis temperature allowed to obtain biochar with a higher specific surface which are consequently more efficient for TCE removal than the ones produced at lower temperature. In our case, biochars P450 and P750 present a similar TCE sorption kinetics. However, they do not present the same specific surface area and pore volume distribution. The total mesopores volume is similar for the two biochars P (0.01 cm^3 g^{-1} for P450 and P750 respectively). However, the total micropores volume is 3 times higher for P750 compare to P450. Hence the increase of the pyrolysis temperature tends to develop the micro-porosity (porosity < 2 nm). Additionally, TCE presents a planar shape with calculated molecular dimensions of 0.66*0.62*0.36 nm. The TCE dimension was determined by Karanfil and Dastgheib (2004) using the molecular dynamics force filed method in PCMODEL version 9 (Serena Software). Consequently, the TCE molecules may not able to penetrate intro ultramicropores (< 0.7 nm). An optimal pore diameter, rather mesoporous pores, seems to be required to enhanced TCE sorption. This is in accordance with other studies which highlighted that highly mesoporous carbonaceous adsorbents were more efficient than microporous sorbents (Lian et al., 2012). Hence, from an economical point of view, it is interesting to notice that the pyrolysis temperature should be carefully set to obtain the most efficient biochar with the lowest energy cost as possible.

3.2.2. Influence of the biochars particles size on TCE remediation

Fig. 4 compares TCE adsorption efficiency according to the particles size distribution for the biochar P750, the most efficient biochar tested. Four classes of particles have been examined: 50 - 100, 100 - 500, 500 - 1000 and 1000 - 2000 µm (distribution is presented in Table 5).

The use of smaller particles size enhanced the sorption kinetic for TCE. The two biggest classes of particles show the less efficient TCE adsorption. After 30 min, 65% of TCE was removed against 90% for the medium class (100 - 500 µm). The best performances however were observed for particles with a diameter lower than 100 µm with 90% of TCE removal in 10 minutes.

Table 5: kinetic parameters for the TCE removal by different particle size distribution (µm) of P750.

		PFO			**PSO**			**IPD**	
Size distribution	q_{exp}	k_1	q_e	R^2	k_2	q_e	R^2	k_{id}	R^2
50 - 100	0.104	0.016	0.016	0.2982	4.88	0.104	0.9998		0.3467
100 - 500	0.105	0.044	0.058	0.8045	2.21	0.107	0.9997		0.5820
500 - 1000	0.105	0.017	0.073	0.8605	0.52	0.110	0.9980		0.8075
1000 - 2000	0.103	0.032	0.085	0.9913	0.77	0.107	0.9992		0.7104

q_{exp} and q_e: mmol g^{-1} k_1: min^{-1} k_2: g $mmol^{-1}.min^{-1}$ k_{id}: $min^{-0.5}$

The TCE kinetics can successfully be fitted with the PSO (R^2: >0.998) but only the fraction 1000 – 2000 µm exhibits a good fit with the PFO (R^2: 0.9913). This tends to indicate that the sorption is limited by the number of active site on the biochar (Mohammed et al., 2018). The IPD model did not fit the kinetic data. As shown in additional files, however, the data can be fitted with two linear plots, which indicates that several mechanisms could influence the sorption. The first linear plot can represent the influence of the external resistance to the mass transfer which is also dependent from the adsorbent particle size among other parameters (Erto et al., 2013). The second can represent the influence of the intraparticle diffusion on the sorption (Fierro et al., 2008). As observed in Fig. 4, decreasing the particle size increase the PFO constant, highlighting thus the increase of the kinetic rate. This result is of great importance since it shows the competitiveness of poplar wood biochars for these kind of applications. In fact, Luo et al. (2016) estimated at 0.35 g $mmol^{-1}$ min^{-1} the TCE uptake on green synthesised agarose-Fe nanoparticles hydrogel at 20°C using the PSO model. Xin et al (2015) tested xanthan gum-modified microscale zero-valent iron particles for TCE, adsorption but they did not present calculations of kinetics constants.

3.2.3. TCE sorption isotherm

Compared to the other biochar, P750 showed the best remediation property for TCE. Additionally, the particle size fraction 50 – 100 µm exhibited the higher sorption rate. Consequently, this fraction was described using sorption isotherm (Fig. 5).

The sorption isotherm of TCE onto biochar P750 exhibits two steps that can be fitted using the Langmuir model. The two steps can be representative of different adsorption sites present at the biochar surface or the possible TCE multilayer adsorption of TCE (Liu, 2015). The biochar presents a maximum sorption capacity of 746 mg g^{-1}. Biochar originating from pine needle exhibited maximum sorption capacity between 90 and 113 $mg.g^{-1}$ depending the pyrolysis temperature (Ahmad et al., 2013b).

3.3. Remediation of groundwater polluted by various Cl-VOCs

The biochar was tested for the remediation of a groundwater sample contaminated by various chlorinated volatile organic compounds (Cl-VOCs) identified in Table 1. Additionally, the biochar was compared to an activated carbon powder used for water de-contamination (Norit SAE Super activated carbon powder). The Cl-VOCs properties and contaminant concentrations are also visible in Table 1. The water sample contained amongst other contaminants trans 1,2-dichloroethylene and tetrachloromethane but at concentration lower than the quantification limit of the method (50 µg L^{-1}). The Cl-VOCs concentration ranged from 130 µg L^{-1} (trichloromethane, TCM) to 96 mg L^{-1} (1,2-cis-dichloroethylene, 1,2-cis-DCE) and contains 49 mg L^{-1} of TCE. Fig. 6 shows the adsorption kinetic with P750 or AC for various organic products in the polluted groundwater sample. It appears that Cl-VOCs exhibit different behaviour with the biochar or the activated carbon powder. Trichloromethane (TCM) is not included in the Fig. 6 for the activated carbon powder due to be under quantification limit after 15 min (< 50 µg L^{-1}).

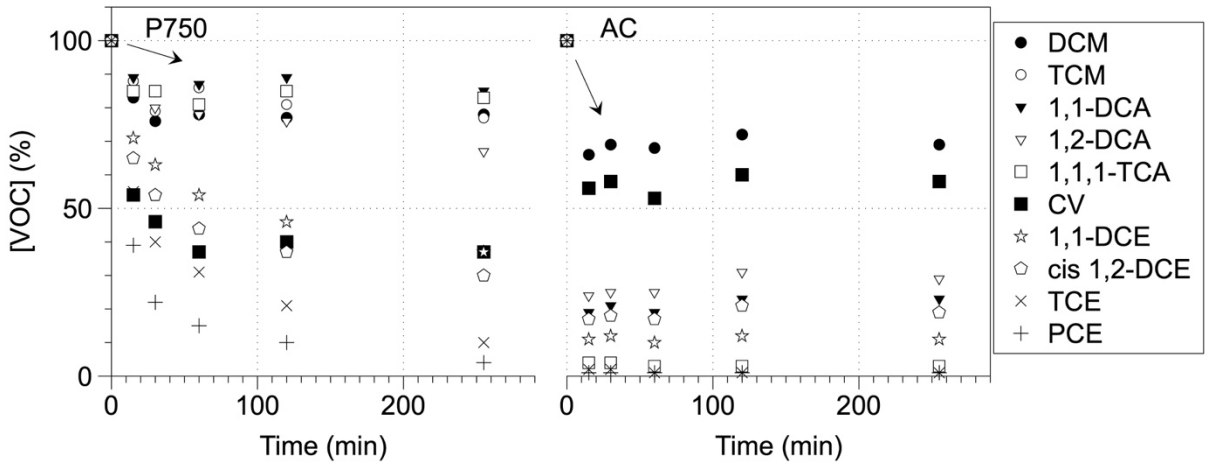

Figure 1: adsorption kinetic of groundwater polluted by chlorinated volatile organic compounds (Cl-VOCs) (Table 1) on biochar P750 (particle size fraction: 50 - 100 µm) and activated carbon powder (AC).

The sorption efficiency varies in the following order:

- For biochar P750

PCE > TCE > cis 1,2DCE > CV = 1,1DCE > 1,2DCA > DCM > TCM > 1,1,1TCA > 1,1DCA

- For activated carbon powder

TCE = PCE > 1,1,1TCA > 1,1DCE > cis 1,2DCE > 1,1DCA > 1,2DCA > CV > DCM

For the biochar, the higher removal rate is obtained for the PCE and the TCE which is in accordance with the high octanol-water partition coefficient (K_{ow}) values of these molecules. The molecules parameters as the K_{ow} is known to significantly impact the sorption efficiency with higher sorption rate for molecules presenting higher K_{ow} (Chen et al., 2018). On another hand, cis 1,2-DCE is more highly removed than 1,1-DCE despite that 1,1-DCE exhibits a higher K_{ow} value. This is potentially due to the competition phenomenon between both molecules, the concentration of cis 1,2-DCE being forty times higher. It is also noticeable that substituted double C=C bounding (ethene) molecules are preferentially sorbed over single bounding C-C (methane and ethane) despite the high concentration of the single bounding C-C 1,1,1-TCA (57 mg L^{-1}). Single C-C molecules adsorption does not exceed 30% at 250 minutes whereas double C=C bounding molecules adsorption is comprised between 60 and 90%. The TCE kinetic rate, when compared with the TCE alone, shows a decrease. Whereas the equilibrium is reached after 30 min for TCE alone, more than 250 min are needed to reach

the equilibrium for TCE in a mixture of other pollutant. This highlighted the importance of the real conditions for the design of water treatments. Additionally, the sorption isotherm showed a maximum sorption at 746 mg g^{-1} for TCE (Fig. 5). After reaching the equilibrium state, the biochar adsorbed 752 mg g^{-1} which is close to the value obtained with the sorption isotherm. However, this demonstrated that despite the biochar sorbed its maximum amount of TCE, it still able to adsorb the others Cl-VOCs. Despite a possible competition for the sorption sites, the Cl-VOCs sorption behaviour can also be control by different phenomena as the steric effect (due to the pore and molecule sizes) and the specific interactions (Schreiter et al., 2018).

Concerning the activating carbon powder, the sorption capacity increase with increasing the K_{ow} values, K_{ow} known to be an important parameter in the molecule behaviour (Chen et al., 2018). Due to its high SSA, the competition between Cl-VOCs is not a preponderant phenomenon. In fact, adsorption stationary state is observed after 15 minutes. In addition, for most of the molecules tested, adsorption reaches at least 70% from after 15 minutes except for dichloromethane and vinyl chlorine, the two less substituted molecules. Another important observation is that biochar is more efficient for vinyl chloride adsorption than activated carbon. At the end of the adsorption test, 65% of vinyl chloride has been removed by biochars whereas only 40% by activated carbon.

4. Conclusions

Among the four studied biochars, the largest surface area was obtained for biochar P750 (341 m^2/g). An increase of the pyrolysis temperature decreases the particle size. P750 presented the highest carbon content (94.7%). T450 exhibited the higher cation exchange capacity. XPS data confirmed that oxygen-bearing functional groups (C-0 and C=O) were in lower quantity at 750°C. TCE adsorption kinetics with PFO and PSO models were proposed. The calculated amount of TCE sorbed were better estimated using the PSO model. Both physisorption and chemisorption were involved in the sorption mechanism for biochars P and T. The particle size fraction (50-100 μm) exhibited the higher sorption ratio for P750. Biochars P are finally the most efficient for TCE removal due to their higher porosity. P750 adsorbed 80% of TCE in 60 min and stabilised 98% of TCE after 250 min with smaller fraction presenting higher kinetic sorption rate. Tests on groundwater polluted by several Cl-VOCs showed that biochar is more efficient to adsorb substituted double C=C boundings molecules rather than single bounding C-C whereas sorption order follows the Cl-VOCs K_{ow} values for the activated carbon powder (AC). Additionally, P750 presents a TCE sorption capacity similar (746 mg g^{-1}) whereas its use in pure TCE solution or in the polluted groundwater. P750 exhibited higher removal capacity for vinyl chloride than the AC.

Acknowledgements

The presented study was associated with CARBOREM project. Financial support was given by BPI France and FEDER (European Funds). The authors acknowledge for the financial support of CARBOREM.

The authors acknowledge Biobasic Environnement for the chlorinated contaminated real groundwater sample.

References

Ahmad, M., Lee, S.S., Dou, X., Mohan, D., Sung, J.-K., Yang, J.E., Ok, Y.S., 2012. Effects of pyrolysis temperature on soybean stover- and peanut shell-derived biochar properties and TCE adsorption in water. Bioresour. Technol. 118, 536–544. https://doi.org/10.1016/j.biortech.2012.05.042

Ahmad, M., Lee, S.S., Oh, S.-E., Mohan, D., Moon, D.H., Lee, Y.H., Ok, Y.S., 2013a. Modeling adsorption kinetics of trichloroethylene onto biochars derived from soybean stover and peanut shell wastes. Environ. Sci. Pollut. Res. 20, 8364–8373. https://doi.org/10.1007/s11356-013-1676-z

Ahmad, M., Lee, S.S., Rajapaksha, A.U., Vithanage, M., Zhang, M., Cho, J.S., Lee, S.-E., Ok, Y.S., 2013b. Trichloroethylene adsorption by pine needle biochars produced at various pyrolysis temperatures. Bioresour. Technol. 143, 615–622. https://doi.org/10.1016/j.biortech.2013.06.033

Ahmad, M., Rajapaksha, A.U., Lim, J.E., Zhang, M., Bolan, N., Mohan, D., Vithanage, M., Lee, S.S., Ok, Y.S., 2014. Biochar as a sorbent for contaminant management in soil and water: A review. Chemosphere 99, 19–33. https://doi.org/10.1016/j.chemosphere.2013.10.071

Ali, I., Asim, Mohd., Khan, T.A., 2012. Low cost adsorbents for the removal of organic pollutants from wastewater. J. Environ. Manage. 113, 170–183. https://doi.org/10.1016/j.jenvman.2012.08.028

Bogusz, A., Oleszczuk, P., Dobrowolski, R., 2015. Application of laboratory prepared and commercially available biochars to adsorption of cadmium, copper and zinc ions from water. Bioresour. Technol. 196, 540–549. https://doi.org/10.1016/j.biortech.2015.08.006

Bolster, C.H., Hornberger, G.M., 2007. On the Use of Linearized Langmuir Equations. Soil Sci. Soc. Am. J. 71, 1796–1806. https://doi.org/10.2136/sssaj2006.0304

Chen, W., Wei, R., Ni, J., Yang, L., Qian, W., Yang, Y., 2018. Sorption of chlorinated hydrocarbons to biochars in aqueous environment: Effects of the amorphous carbon structure of biochars and the molecular properties of adsorbates. Chemosphere 210, 753–761. https://doi.org/10.1016/j.chemosphere.2018.07.071

De Gisi, S., Lofrano, G., Grassi, M., Notarnicola, M., 2016. Characteristics and adsorption capacities of low-cost sorbents for wastewater treatment: A review. Sustainable Mater. Technol. 9, 10–40. https://doi.org/10.1016/j.susmat.2016.06.002

Erto, A., Andreozzi, R., Lancia, A., Musmarra, D., 2010. Factors affecting the adsorption of trichloroethylene onto activated carbons. Appl. Surf. Sci. 256, 5237–5242. https://doi.org/10.1016/j.apsusc.2009.12.110

Erto, A., Lancia, A., Musmarra, D., 2013. Fixed-bed adsorption of trichloroethylene onto activated carbon. Chemical Engineering Transactions 32. https://doi.org/10.3303/CET1332329

Fierro, V., Torné-Fernández, V., Montané, D., Celzard, A., 2008. Adsorption of phenol onto activated carbons having different textural and surface properties. Microporous and Mesoporous Mater. 111, 276–284. https://doi.org/10.1016/j.micromeso.2007.08.002

Fiol, N., Villaescusa, I., 2009. Determination of sorbent point zero charge: usefulness in sorption studies. Environ. Chem. Lett 7, 79–84. https://doi.org/10.1007/s10311-008-0139-0

Genthe, B., Kapwata, T., Le Roux, W., Chamier, J., Wright, C.Y., 2018. The reach of human health risks associated with metals/metalloids in water and vegetables along a contaminated river catchment: South Africa and Mozambique. Chemosphere 199, 1–9. https://doi.org/10.1016/j.chemosphere.2018.01.160

Harvey, O.R., Herbert, B.E., Rhue, R.D., Kuo, L.-J., 2011. Metal Interactions at the Biochar-Water Interface: Energetics and Structure-Sorption Relationships Elucidated by Flow Adsorption Microcalorimetry. Environ. Sci. Technol. 45, 5550–5556. https://doi.org/10.1021/es104401h

Karanfil, T., Dastgheib, S.A., 2004. Trichloroethylene Adsorption by Fibrous and Granular Activated Carbons: Aqueous Phase, Gas Phase, and Water Vapor Adsorption Studies †. Environ. Sci. Technol. 38, 5834–5841. https://doi.org/10.1021/es0497936

Khan, S., Priyamvada, S., Khan, S.A., Khan, W., Farooq, N., Khan, F., Yusufi, A.N.K., 2009. Effect of trichloroethylene (TCE) toxicity on the enzymes of carbohydrate metabolism, brush border membrane and oxidative stress in kidney and other rat tissues. Food Chem. Toxicol. 47, 1562–1568. https://doi.org/10.1016/j.fct.2009.04.002

Kushwaha, A., Hans, N., Kumar, S., Rani, R., 2018. A critical review on speciation, mobilization and toxicity of lead in soil-microbe-plant system and bioremediation strategies. Ecotoxicol. Environ. Saf. 147, 1035–1045. https://doi.org/10.1016/j.ecoenv.2017.09.049

Lam, S.S., Liew, R.K., Lim, X.Y., Ani, F.N., Jusoh, A., 2016. Fruit waste as feedstock for recovery by pyrolysis technique. Int. Biodeterior. Biodegrad. 113, 325–333. https://doi.org/10.1016/j.ibiod.2016.02.021

Largitte, L., Pasquier, R., 2016. A review of the kinetics adsorption modelsand their application to the adsorption of lead by an activated carbon. Chem. Eng. Res. Des. 109, 495–504.

Lehmann, J., 2007. Bio-energy in the black. Front. Ecol. Environ. 5, 381–387.

Li, H., Dong, X., da Silva, E.B., de Oliveira, L.M., Chen, Y., Ma, L.Q., 2017. Mechanisms of metal sorption by biochars: Biochar characteristics and modifications. Chemosphere 178, 466–478. https://doi.org/10.1016/j.chemosphere.2017.03.072

Lian, F., Chang, C., Du, Y., Zhu, L., Xing, B., Liu, C., 2012. Adsorptive removal of hydrophobic organic compounds by carbonaceous adsorbents: A comparative study of waste-polymer-based, coal-based activated carbon, and carbon nanotubes. J. Environ. Sci. 24, 1549–1558. https://doi.org/10.1016/S1001-0742(11)60984-4

Liu, S., 2015. Cooperative adsorption on solid surfaces. J. Colloid Interface Sci. 450, 224–238. https://doi.org/10.1016/j.jcis.2015.03.013

Loflen, C.L., Buck, T., Bonnema, A., Heim, W.A., 2018. Pollutant bioaccumulation in the California spiny lobster (Panulirus interruptus) in San Diego Bay, California, and potential human health implications. Mar. Pollut. Bull. 128, 585–592. https://doi.org/10.1016/j.marpolbul.2018.02.001

Luo, F., Chen, Z., Megharaj, M., Naidu, R., 2016. Simultaneous removal of trichloroethylene and hexavalent chromium by green synthesized agarose-Fe nanoparticles hydrogel. Chem. Eng. J. 294, 290–297. https://doi.org/10.1016/j.cej.2016.03.005

Mohammed, N.A.S., Abu-Zurayk, R.A., Hamadneh, I., Al-Dujaili, A.H., 2018. Phenol adsorption on biochar prepared from the pine fruit shells: Equilibrium, kinetic and thermodynamics studies. J. Environ. Manage. 226, 377–385. https://doi.org/10.1016/j.jenvman.2018.08.033

Saleh, S., Kamarudin, K.B., Ghani, W.A.W.A.K., Kheang, L.S., 2016. Removal of Organic Contaminant from Aqueous Solution Using Magnetic Biochar. Procedia Eng. 148, 228–235. https://doi.org/10.1016/j.proeng.2016.06.590

Schreiter, I.J., Schmidt, W., Schüth, C., 2018. Sorption mechanisms of chlorinated hydrocarbons on biochar produced from different feedstocks: Conclusions from single- and bi-solute experiments. Chemosphere 203, 34–43. https://doi.org/10.1016/j.chemosphere.2018.03.173

Siggings, A., Abram, F., Healy, M.G., 2020. Pyrolysed waste materials show potential for remediation of trichloroethylene-contaminated water. J. Hazard. Mater. 390, 121909. https://doi.org/10.1016/j.jhazmat.2019.121909

Smith, M., Scudiero, L., Espinal, J., McEwen, J.-S., Garcia-Perez, M., 2016. Improving the deconvolution and interpretation of XPS spectra from chars by ab initio calculations. Carbon 110, 155–171. https://doi.org/10.1016/j.carbon.2016.09.012

Tan, X., Liu, Y., Zeng, G., Wang, X., Hu, X., Gu, Y., Yang, Z., 2015. Application of biochar for the removal of pollutants from aqueous solutions. Chemosphere 125, 70–85. https://doi.org/10.1016/j.chemosphere.2014.12.058

Trakal, L., Bingöl, D., Pohořelý, M., Hruška, M., Komárek, M., 2014. Geochemical and spectroscopic investigations of Cd and Pb sorption mechanisms on contrasting biochars: Engineering implications. Bioresour. Technol. 171, 442–451. https://doi.org/10.1016/j.biortech.2014.08.108

Trama-Freitas, B., Freitas, J.C.S., Martins, R.C., Gando-Ferreira, L.M., Quinta-Ferreira, M.E., Quinta-Ferreira, R.M., do Carmo, D.R., 2017. A study of bio-hybrid silsesquioxane/yeast: Biosorption and neuronal toxicity of lead. J. Biotechnol. 264, 43–50. https://doi.org/10.1016/j.jbiotec.2017.10.015

Xin, J., Han, J., Zheng, X., Shao, H., Kolditz, O., 2015. Mechanism insights into enhanced trichloroethylene removal using xanthan gum-modified microscale zero-valent iron particles. J. Environ. Manage. 150, 420–426. https://doi.org/10.1016/j.jenvman.2014.12.022

Yaashikaa, P.R., Senthil Kumar, P., Varjani, S.J., Saravanan, A., 2019. Advances in production and application of biochar from lignocellulosic feedstocks for remediation of environmental pollutants. Bioresourc. Technol. 192, 122030. https://doi.org/10.1016/j.biortech.2019.122030

Zhang, C., Feng, Y., Liu, Y., Chang, H., Li, Z., Xue, J., 2017. Uptake and translocation of organic pollutants in plants: A review. J. Integr. Agric. 16, 1659–1668. https://doi.org/10.1016/S2095-3119(16)61590-3

FIGURES

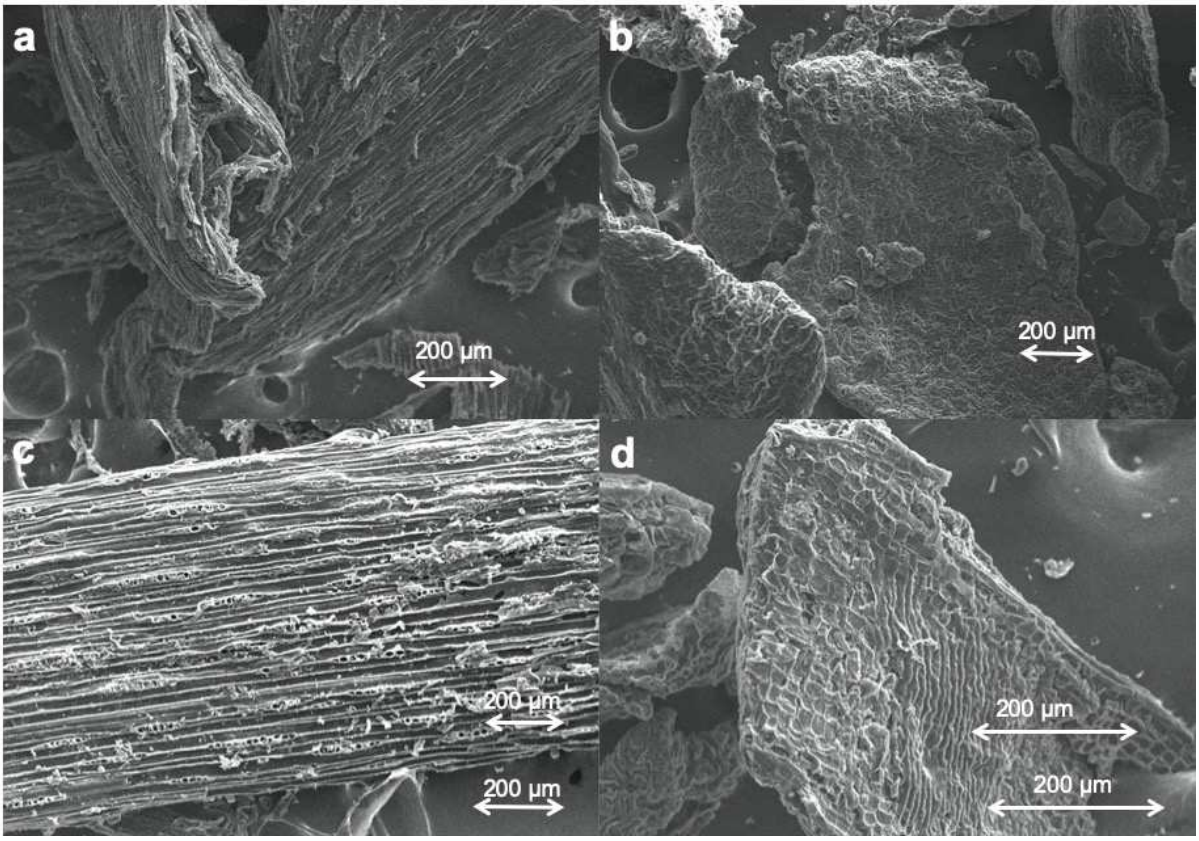

Figure 1. Scanning electron microscopy of biochar produced at 450°C from (**a**) poplar wood (P450) and (**b**) tea (T450) and at 750°C from (**c**) poplar wood (P750) and (**d**) tea (T750).

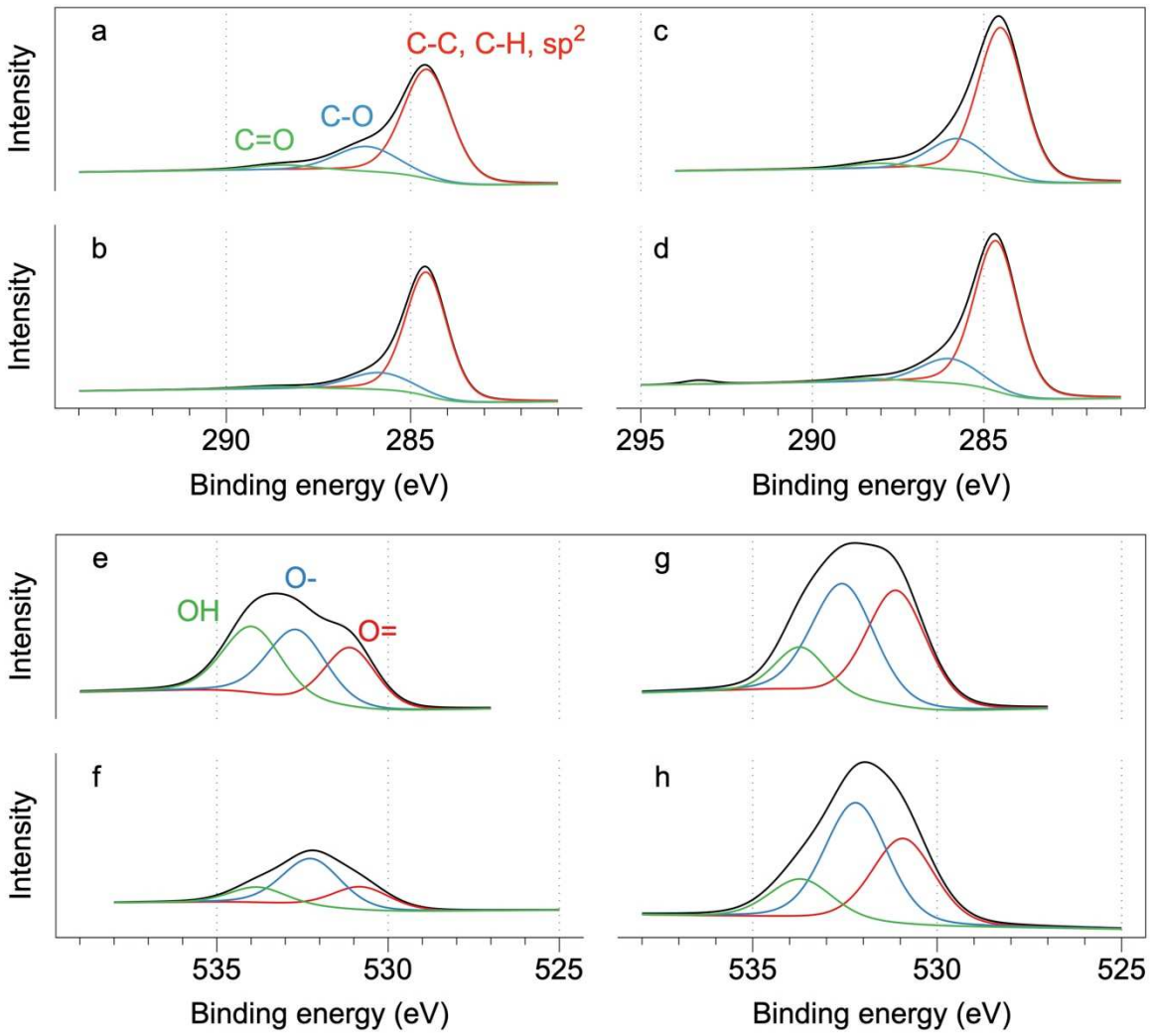

Figure 2. XPS high resolution survey scans of C1s (**a**,**b**,**c**,**d**) and O1s (**e**,**f**,**g**,**h**) region of (**a**,**e**), poplar wood biochar prepared at 450°C (P450) and (**b**,**f**) 750°C (P750), (**c**,**g**) tea biochar prepared at 450°C (T450) and (**d**,**h**) 750°C (T750).

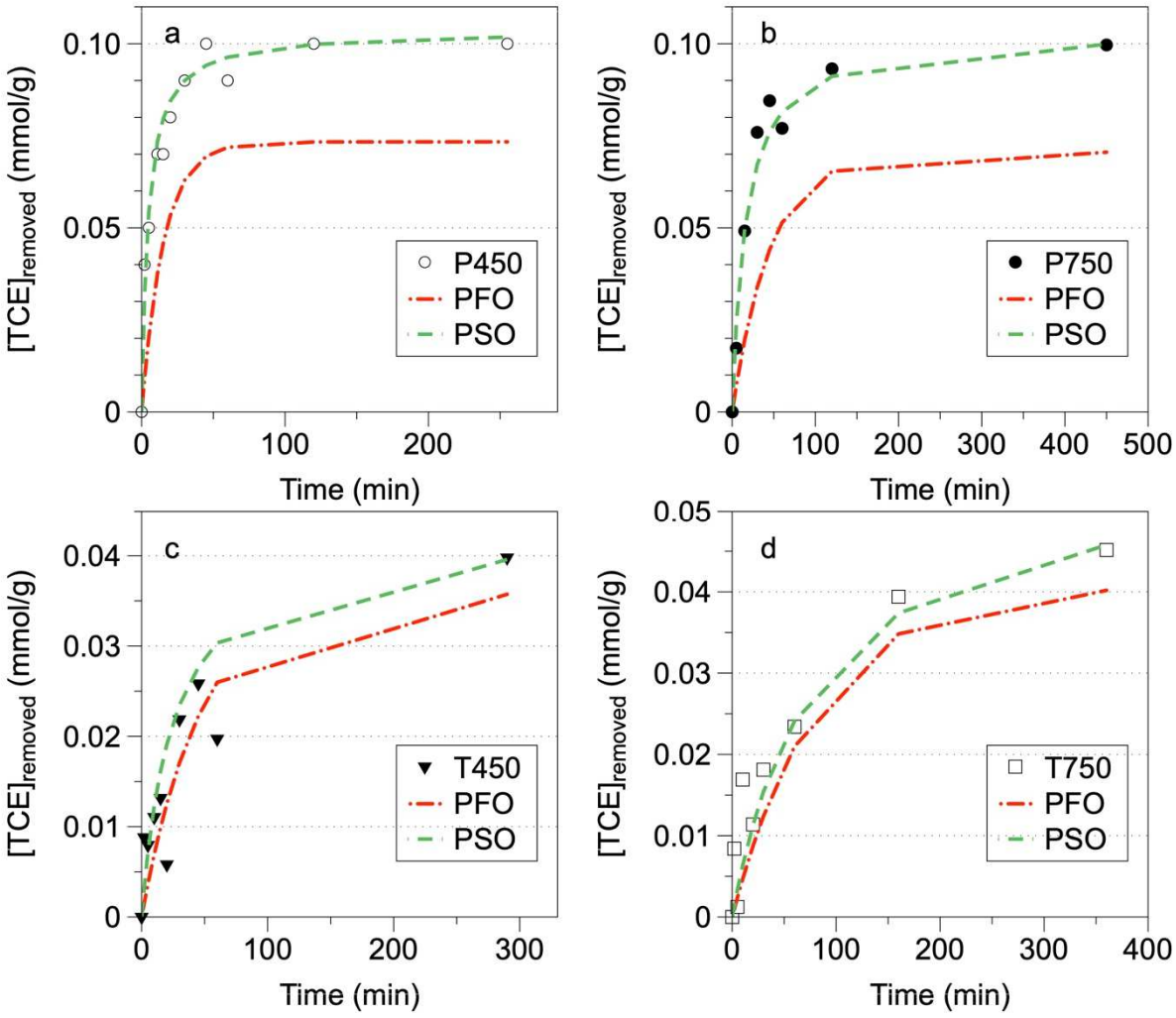

Figure 3. Trichloroethylene (TCE) adsorption kinetic to (**a**) poplar wood biochar prepared at 450°C (P450) and (**b**) 750°C (P750), (**c**) tea biochar prepared at 450°C (T450) and (**d**) 750°C (T750). Each data sets were modelled using pseudo-first order (PFO) and pseudo-second order (PSO).

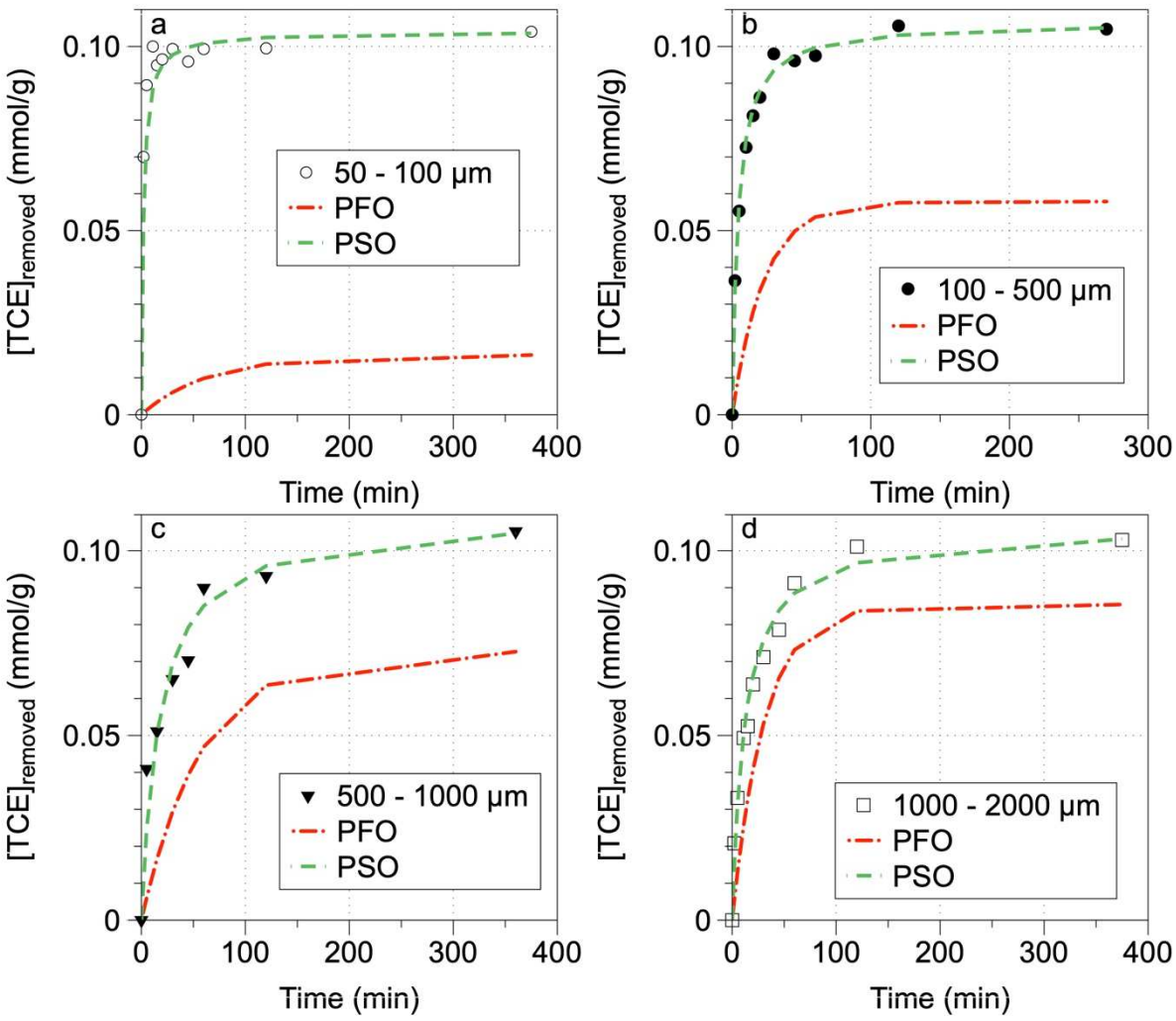

Figure 4. Trichloroethylene (TCE) adsorption kinetic on different particle size distribution of biochar P750. (**a**) 50 to 100 µm, (**b**) 100 to 500 µm, (**c**) 500 to 1000 µm and (**d**) 1000 to 2000 µm. Each data sets were modelled using pseudo-first order (PFO) and pseudo-second order (PSO).

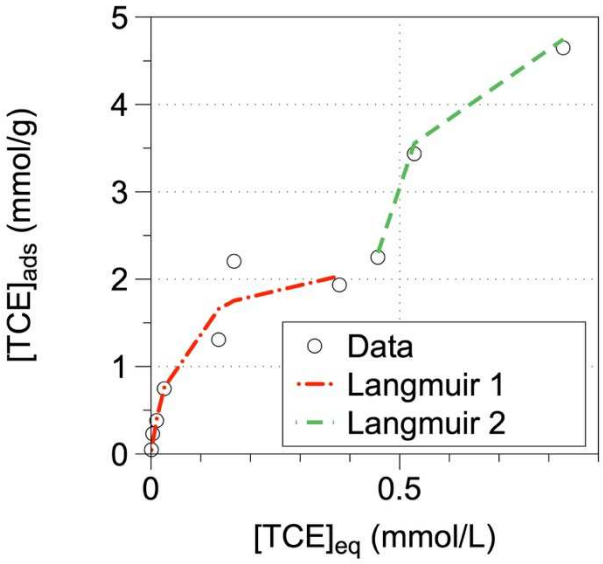

	Langmuir 1	Langmuir 2
K (L $mmol^{-1}$)	18.4	11.3
Smax (mmol g^{-1})	2.33	3.35
K (L mg^{-1})	0.14	0.086
Smax (mg g^{-1})	306	440
R^2	0.9870	0.9990

Figure 5. Sorption isotherm of trichloroethylene (TCE) to poplar wood biochar prepared at 750°C (P750) (particle size 50 – 100 µm). Data were fitted with the Langmuir model.

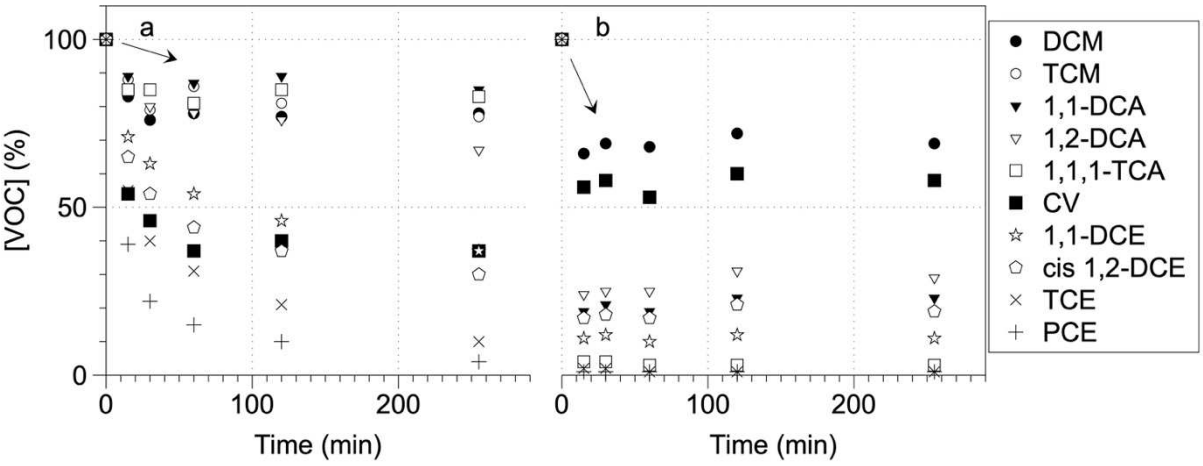

Figure 6. Adsorption kinetic of groundwater polluted by various chlorinated volatile organic compounds (Cl-VOCs) (Table S1) on (**a**) poplar wood biochar prepared at 750°C (P750) (particle size fraction: 50 - 100 µm) and (**b**) activated carbon powder.